THE JOURNAL OF PHYSICAL CHEMISTRY C

Article

pubs.acs.org/JPCC

Anion Photoelectron Spectroscopy and Theoretical Investigation on $Nb_2Si_n^{-/0}$ (n = 2−12) Clusters

Sheng-Jie Lu,[†,‡] Hong-Guang Xu,*[,†,‡] Xi-Ling Xu,*[,†,‡] and Wei-Jun Zheng*[,†,‡]

[†]Beijing National Laboratory for Molecular Sciences (BNLMS), State Key Laboratory of Molecular Reaction Dynamics, Institute of Chemistry, Chinese Academy of Sciences, Beijing 100190, China

[‡]University of Chinese Academy of Sciences, Beijing 100049, China

Supporting Information

ABSTRACT: We measured the photoelectron spectra of $Nb_2Si_n^-$ (n = 2−12) anions and investigated the geometric structures and electronic properties of $Nb_2Si_n^-$ anions and their neutral counterparts with ab initio calculations. The most stable structures of $Nb_2Si_n^{-/0}$ (n = 2−12) clusters can be regarded as a central axis of Nb_2 surrounded by the Si atoms. The most stable isomers of $Nb_2Si_n^-$ anions are in spin doublet states, while those of the neutral clusters are in spin singlet states. The results showed that the two Nb atoms in $Nb_2Si_n^{-/0}$ clusters incline to form a strong Nb−Nb bond and also prefer to occupy the high coordination sites to form more Nb−Si bonds. The most stable isomers of anionic and neutral Nb_2Si_3 are D_{3h}-symmetric trigonal bipyramid structures, and that of $Nb_2Si_6^-$ has C_{2h} symmetry with the six Si atoms forming a chair-shaped structure. The ground state structure of the $Nb_2Si_{12}^-$ anion is a C_{6v}-symmetric capped hexagonal antiprism in which one Nb atom is encapsulated inside the Si_{12} cage and the second Nb atom caps the top of the hexagonal antiprism. It is found that the atomic dipole moment-corrected Hirshfeld population (ADCH) charge distributions on the two Nb atoms not only depend on the electronegativities of Si and Nb atoms but also relate with the structural evolution of $Nb_2Si_n^-$ clusters. The molecular orbital analyses of $Nb_2Si_3^-$, $Nb_2Si_6^-$, and $Nb_2Si_{12}^-$ anions indicate that the delocalized Nb_2−Si_n ligand interactions and the strong Nb−Nb bonds play important roles in their structural stability.

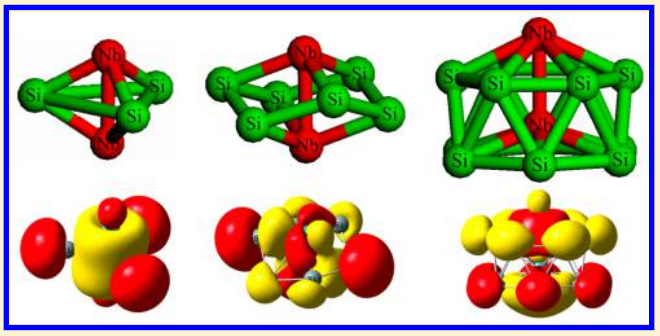

INTRODUCTION

Silicon is widely used in modern microelectronics devices. Many experimental and theoretical works have been conducted to understand the structures and properties of transition-metal (TM) doped silicon clusters because these clusters not only are useful for silicon-based catalysts, solar cells, and lithium-ion baterries[1−7] but also can be used as building blocks of cluster-assembled materials.[8−12] Compared to single-TM atom-doped silicon clusters, multiple-TM atom-doped silicon clusters may hold very special geometric structures such as tubular, pearl-chain style, wheel-like, stacked naphthalene-like, or dodecahedral structures[13−18] and have special magnetic properties such as ferromagnetism or antiferromagnetism.[12,15,19−22]

Niobium-doped silicon clusters have attracted great attention because niobium is widely used in the alloy industry and superconducting materials. Amorphous thin Nb_xSi_{1-x} films can be used to probe the mechanisms of superconductor−insulator transitions (SIT).[23−26] Niobium silicide films or alloys can be used in digital superconducting electronics (SCE)[27] and in bolometers for astrophysical particle detection.[28−31] Nb−Si-based superalloys may be used as high-temperature materials in aircraft turbine engines and rockets because of their excellent mechanical properties at high temperature.[32−40] The structures of silicon clusters doped with one or two Nb atoms have been studied previously by several theoretical calculations.[41−48] The diatomic $NbSi^-$ anion was studied by photoelectron imaging experiments and ab initio calculations,[49] and the $NbSi_n^-$ anions in the size range of n = 3−18 were investigated with anion photoelectron spectroscopy.[50,51] The $NbSi_n^+$ (n = 6−20) and $Nb_2Si_n^+$ (n = 13−19) cations were studied with mass spectrometry and H_2O adsorption reactivity experiments.[52] The $NbSi_n^+$ (n = 4−12) cations were also investigated using argon-tagged infrared multiphoton dissociation (IR-MPD) experiments and density functional theory (DFT) calculations.[53] In order to get more detailed information regarding the geometric structures and electronic properties of Nb_2Si_n clusters, in this work we investigated $Nb_2Si_n^{-/0}$ (n = 2−12) clusters with size-selected anion photoelectron spectroscopy and ab initio calculations. It is found that the two Nb atoms in $Nb_2Si_n^{-/0}$ clusters form a strong Nb−Nb bond and the $Nb_2Si_3^{-/0}$, $Nb_2Si_6^-$, and $Nb_2Si_{12}^-$ clusters have high symmetric geometric structures.

Received: February 27, 2017
Revised: May 5, 2017
Published: May 8, 2017

DOI: 10.1021/acs.jpcc.7b01904
J. Phys. Chem. C 2017, 121, 11851−11861

EXPERIMENTAL AND THEORETICAL METHODS

Experimental Method. The experiments were conducted on a home-built apparatus consisting of a laser vaporization cluster source, a time-of-flight mass spectrometer, and a magnetic-bottle photoelectron spectrometer, which has been described elsewhere.[54] The $Nb_2Si_n^-$ cluster anions were produced with the laser vaporization source by laser ablation of a rotating and translating Nb/Si disk target (Nb:Si mole ratio 1:1, 13 mm diameter) with the second-harmonic light (532 nm) pulses from a nanosecond Nd:YAG laser (Continuum Surelite II-10), while helium carrier gas with ∼0.4 MPa backing pressure was allowed to expand through a pulsed valve (General Valve Series 9) into the source to cool the $Nb_2Si_n^-$ clusters. The clusters anions were mass analyzed by the time-of-flight mass spectrometer. The $Nb_2Si_n^-$ anions were each size selected with a mass gate and decelerated by a momentum decelerator before crossing with the laser beam of the fourth-harmonic light (266 nm) pulses from the other Nd:YAG laser at the photodetachment region. The resulting electrons were energy analyzed by the magnetic-bottle photoelectron spectrometer. The photoelectron spectra were calibrated with the spectra of Cu^- and Au^- ions taken under similar conditions. The resolution of the magnetic-bottle photoelectron spectrometer was about 40 meV for electrons with 1 eV kinetic energy.

Theoretical Method. Full structural optimizations and frequency analyses of $Nb_2Si_n^-$ anions and their neutral counterparts were carried out employing density functional theory (DFT) with the Beck's three-parameter and Lee−Yang−Parr's gradient-corrected correlation hybrid functional (B3LYP),[55,56] as implemented in the Gaussian 09 program package.[57] The exchange-correlation potential and effective core pseudopotential LanL2DZ basis set[58] was used for the Nb atoms, and the Pople's all-electron 6-311+G(d) basis set[59] was used for the Si atoms. No symmetry constraint was imposed during the geometry optimizations for both anionic and neutral clusters. For all clusters, numerous initial structures reported in the literature were taken into accounts at all possible spin states. Additionally, the swarm-intelligence-based CALYPSO structure prediction software[60] was used to search the global minima for both anionic and neutral clusters. CALYPSO is an efficient structure prediction method. This approach requires only chemical compositions for a given cluster to predict stable or metastable structures at given external conditions. The success of CALYPSO is due to the integration of several major techniques, which include structural evolution through PSO algorithm, symmetry constraint during structure generation, the Metropolis criterion, atom-centered symmetrical function, and bond characterization matrix (BCM). These critical techniques can enhance the capability of CALYPSO in dealing with more complex systems and can also accelerate the structural optimization process, reduce searching space, enhance the structural diversity, and eliminate similar structures on the potential energy surfaces to enhance searching efficiency. Harmonic vibrational frequency analyses were performed to verify that the optimized structures are the true minima on the potential energy surfaces. The theoretical vertical detachment energies (VDEs) were calculated as the energy differences between the neutrals and the anions both at the geometries of anionic species, while the theoretical adiabatic detachment energies (ADEs) were calculated as the energy differences between the neutrals and the anions with the neutrals relaxed to the nearest local minima using the geometries of the corresponding anions as initial structures. The single-point energies of $Nb_2Si_{2-12}^{-/0}$ clusters were calculated by using the coupled-cluster methods including single, double, and perturbative triple excitation [CCSD(T)][61,62] to obtain more accurate relative energies of the low-lying isomers in which the aug-cc-pVDZ-PP basis set[63] was used for the Nb atoms and cc-pVDZ basis set[64] was used for the Si atoms. Zero-point energy (ZPE) corrections obtained from the B3LYP functional were included in all calculated energies. To gain insight into the charge distributions of $Nb_2Si_{2-12}^-$ anions, we used the program Multiwfn[65] to conduct the atomic dipole moment-corrected Hirshfeld population (ADCH) analyses. The ADCH charge is proposed by Lu et al.[66] and is an improved version of Hirshfeld charge to resolve many inherent drawbacks of Hirshfeld charge, such as the poor dipole moment reproducibility.[67] Also, it has many advantages over the Mulliken, NPA, and AIM charges in dealing with atomic charge distributions of clusters. The program Multiwfn was also employed to analyze the orbital compositions by using the natural atomic orbital method.

EXPERIMENTAL RESULTS

The photoelectron spectra of $Nb_2Si_n^-$ (n = 2−12) clusters recorded with 266 nm photons are presented in Figure 1, and the experimental VDEs and ADEs of these clusters obtained from their photoelectron spectra are summarized in Table 1. The experimental VDEs of these clusters were estimated from the maxima of the first peaks. We drew a straight line along the rising edge of the first peaks and made the straight line intersect with the baseline of the experimental spectra. The electron binding energy (EBE) values at the intersection points plus the instrumental resolution were assigned as the experimental ADEs.

The experimental peaks in the photoelectron spectra of $Nb_2Si_n^-$ shift to the higher EBE region with increasing number of Si atoms. Due to the existence of the second Nb atom, the spectral features of $Nb_2Si_n^-$ are more complex than those of $NbSi_n^-$ and the VDEs of $Nb_2Si_n^-$ are relatively lower than those of corresponding $NbSi_n^-$.[51]

The photoelectron spectrum of $Nb_2Si_2^-$ reveals five major peaks centered at 1.95, 2.51, 3.06, 3.44, and 3.83 eV, respectively. In the spectrum of $Nb_2Si_3^-$, there is a low-intensity shoulder peak at 2.13 eV, followed by five major peaks centered at 2.52, 2.66, 2.92, 3.50, and 3.91 eV, respectively. The spectrum of $Nb_2Si_4^-$ displays a broad shoulder peak at 2.23 eV and a high-intensity peak at 2.68 eV, followed by four barely resolved broad peaks at 3.23, 3.48, 3.65, and 4.15 eV, respectively. As for the spectrum of $Nb_2Si_5^-$, there are a low-intensity peak centered at 2.37 eV, a high-intensity broad peak centered at 3.19 eV, a shoulder peak between 2.37 and 3.19 eV, a major peak centered at 3.50 eV, followed by two barely distinguishable peaks at 3.95 and 4.20 eV. The spectrum of $Nb_2Si_6^-$ has a low-intensity peak centered at 2.62 eV and three high-intensity peaks centered at 2.98, 3.41, and 3.82 eV. A low-intensity peak centered at 2.71 eV and two high-intensity peaks centered at 3.34 and 3.96 eV can be observed in the spectrum of $Nb_2Si_7^-$.

The spectrum of $Nb_2Si_8^-$ displays a low-EBE tail in the range of 2.4−2.8 eV, a major peak centered at 3.08 eV, and another high-intensity broad peak in the range of 3.25−4.25 eV. The spectrum of $Nb_2Si_9^-$ possesses a low-intensity peak centered at 2.94 eV followed by three barely resolved peaks centered at 3.56, 3.81, and 4.13 eV, respectively. In the spectrum of

DOI: 10.1021/acs.jpcc.7b01904
J. Phys. Chem. C 2017, 121, 11851−11861

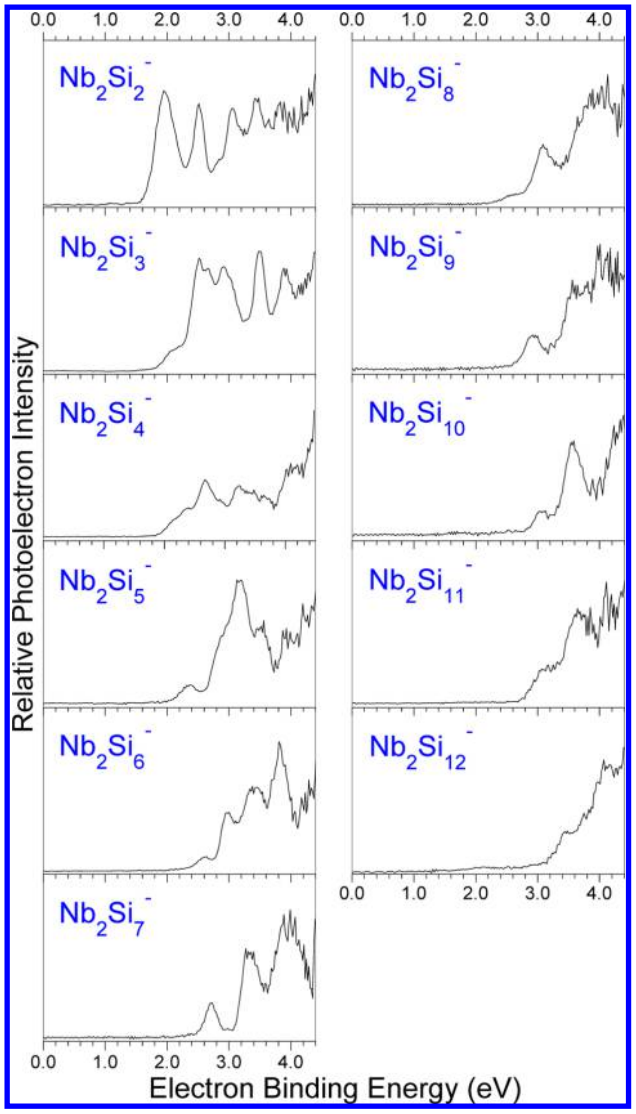

Figure 1. Photoelectron spectra of $Nb_2Si_n^-$ (n = 2−12) clusters recorded with 266 nm photons.

$Nb_2Si_{10}^-$, a low-intensity peak centered at 3.07 eV, a high-intensity peak centered at 3.57 eV, and the onset of the third peak beyond 4.20 eV can be observed. In the spectrum of $Nb_2Si_{11}^-$, three peaks centered at 3.09, 3.67, and 4.11 eV are distinguishable. In the spectrum of $Nb_2Si_{12}^-$, there is a roughly distinguishable peak centered at 3.45 eV followed by two unresolved peaks at 3.75 and 4.06 eV.

THEORETICAL RESULTS

The typical low-lying isomers of $Nb_2Si_n^-$ (n = 2−12) clusters are presented in Figure 2, in which the most stable ones are shown on the left. The relative energies (ΔE) of the low-lying isomers and their theoretical VDEs and ADEs are summarized in Table 1 along with the experimental VDEs and ADEs for comparison. The bond lengths of the most stable isomers of $Nb_2Si_n^{-/0}$ (n = 2−12) clusters are shown in Table 2. In addition, we simulated the photoelectron spectra of the low-lying isomers based on the generalized Koopmans' theorem (GKT).[68,69] We call the simulated spectra density of states (DOS) spectra for convenience. The DOS spectra and experimental photoelectron spectra are compared in Figure 3. In the DOS spectra, each transition is treated equally in the simulations.

$Nb_2Si_n^-$ (n = 2−12) Anions. *$Nb_2Si_2^-$*. The most stable isomer of $Nb_2Si_2^-$ (2A) is a C_{2v}-symmetric tetrahedron structure. Its theoretical VDE (1.81 eV) is in reasonable agreement with the experimental value (1.95 eV), and its simulated DOS spectrum can roughly reproduce the peak positions and patterns of the experimental spectrum, although the intensity of the high EBE part of the DOS spectrum is slightly higher than that of the experimental spectrum. The existence of isomer 2B can be ruled out because it is much higher in energy than isomer 2A by 0.44 eV. Therefore, we suggest that isomer 2A is the most likely structure observed in our experiments.

$Nb_2Si_3^-$. For $Nb_2Si_3^-$, the most stable isomer (3A) is a D_{3h}-symmetric trigonal bipyramid in which each Nb atom is coordinated with three Si atoms. The calculated VDE (2.14 eV) is in excellent agreement with the experimental value (2.13 eV), and its simulated DOS spectrum can roughly reproduce the peak positions and patterns of the experimental spectrum. Isomer 3B is higher in energy than isomer 3A by 0.10 eV. The existence of isomers 3C and 3D can be ruled out because they are much higher in energy than isomer 3A by at least 0.53 eV. Thus, we suggest isomer 3A to be the most probable structure contributing to the photoelectron spectrum of $Nb_2Si_3^-$, and isomer 3B may have some contribution to the higher electron binding energy (EBE) sides of the photoelectron spectrum.

$Nb_2Si_4^-$. The most stable isomer (4A) of $Nb_2Si_4^-$ can be viewed as adding a Si atom to cap the triangular face of isomer 3B. The theoretical VDEs (2.23 and 2.13 eV) of isomers 4A and 4B are both in excellent agreement with the experimental value (2.23 eV), and the energy difference between 4A and 4B is only 0.05 eV. The simulated spectrum of isomer 4A can match most of the experimental peaks, and that of isomer 4B is in reasonable agreement with the experimental peaks at 3.23 and 3.65 eV. The combination of the DOS spectra of isomers 4A and 4B can reproduce the peak positions and patterns of the experimental spectrum. Isomers 4C and 4D are impossible to present in our experiments because they are much higher in energy than isomer 4A by at least 0.30 eV. Thus, isomers 4A and 4B are suggested to be the most probable structures detected in our experiments.

$Nb_2Si_5^-$. As for $Nb_2Si_5^-$, the most stable isomer (5A) can be obtained by an additional Si atom capping the folded rhombic $NbSi_3$ unit of isomer 4A. The theoretical VDE (2.38 eV) of isomer 5A is in excellent agreement with the experimental value (2.37 eV), and its simulated DOS spectrum fits the peak positions and patterns of the experimental spectrum very well. Isomer 5B is higher in energy than isomer 5A by 0.18 eV. The existence of isomers 5C and 5D can be ruled out because they are much higher in energy than isomer 5A by at least 0.66 eV. Thus, we suggest isomer 5A to be the most probable structure contributing to the photoelectron spectrum of $Nb_2Si_5^-$, and isomer 5B may have some contribution to the higher EBE sides of the photoelectron spectrum.

$Nb_2Si_6^-$. The most stable isomer of $Nb_2Si_6^-$ (6A) is of C_{2h} symmetry in which six Si atoms form a chair-shaped structure with each Nb atom interacting with three Si atoms. This structure is similar to that of $V_2Si_6^-$.[54] The calculated VDE (3.14 eV) of isomer 6A is in good agreement with the experimental peak at 2.98 eV, and that (2.62 eV) of isomer 6B is consistent with the experimental peak at 2.62 eV. Isomer 6B is slightly higher in energy than isomer 6A by 0.13 eV. The

DOI: 10.1021/acs.jpcc.7b01904
J. Phys. Chem. C 2017, 121, 11851−11861

Table 1. Relative Energies, Theoretical VDEs and ADEs of the Low-Lying Isomers of $Nb_2Si_n^-$ (n = 2−12) Clusters, and Experimental VDEs and ADEs Estimated from Their Photoelectron Spectra[a]

				VDE (eV)		ADE (eV)						VDE (eV)		ADE (eV)	
	isomer	sym	ΔE^b (eV)/ CCSD(T)	theo.[c]	expt.[d]	theo.[c]	expt.[d]		isomer	sym	ΔE^b (eV)/ CCSD(T)	theo.[c]	expt.[d]	theo.[c]	expt.[d]
$Nb_2Si_2^-$	**2A**	C_{2v}	0.00	1.81	1.95	1.72	1.61	$Nb_2Si_8^-$	**8A**	C_1	0.00	2.99	3.08	2.83	2.76
	2B	C_{2v}	0.44	2.04		1.97			**8B**	C_s	0.07	3.03		2.91	
$Nb_2Si_3^-$	**3A**	D_{3h}	0.00	2.14	2.13	1.84	1.77		**8C**	C_1	0.17	2.96		2.62	
	3B	C_{2v}	0.10	2.46		2.21			**8D**	C_1	0.20	2.73	2.70	2.63	2.32
	3C	C_s	0.53	2.05		1.94		$Nb_2Si_9^-$	**9A**	C_s	0.00	2.97	2.94	2.86	2.62
	3D	C_s	0.73	1.53		1.51			9B	C_s	0.24	2.66		2.54	
$Nb_2Si_4^-$	**4A**	C_1	0.00	2.23	2.23	2.16	1.89		9C	C_1	0.41	2.95		2.74	
	4B	C_1	0.05	2.13		1.97			9D	C_1	0.51	2.99		2.85	
	4C	C_{2v}	0.30	2.76		1.97		$Nb_2Si_{10}^-$	**10A**	C_1	0.00	3.02	3.07	2.81	2.79
	4D	C_1	0.46	2.26		1.99			10B	C_1	0.38	3.08		2.99	
$Nb_2Si_5^-$	**5A**	C_s	0.00	2.38	2.37	2.11	2.00		10C	C_1	0.68	3.10		2.94	
	5B	C_s	0.18	2.77		2.54			10D	C_2	0.98	2.88		2.72	
	5C	C_s	0.66	1.99		1.69		$Nb_2Si_{11}^-$	**11A**	C_s	0.00	3.07	3.09	2.74	2.75
	5D	C_s	0.73	2.09		2.01			11B	C_1	0.03	2.96		2.76	
$Nb_2Si_6^-$	**6A**	C_{2h}	0.00	3.14	2.98	2.84	2.77		11C	C_1	0.21	3.00		2.75	
	6B	C_1	0.13	2.62	2.62	2.48	2.28		11D	C_1	0.46	2.90		2.73	
	6C	C_1	0.32	2.56		2.31		$Nb_2Si_{12}^-$	**12A**	C_{6v}	0.00	3.41	3.45	3.32	3.18
	6D	C_{2v}	0.33	3.10		2.28			12B	C_1	0.04	2.99		2.84	
$Nb_2Si_7^-$	**7A**	C_1	0.00	2.71	2.71	2.61	2.50		12C	C_2	0.09	3.32		2.81	
	7B	C_1	0.48	2.64		2.46			12D	C_1	0.93	3.25		3.16	
	7C	C_1	0.67	2.82		2.56									
	7D	C_1	0.94	2.62		2.43									

[a]The isomers labeled in bold are the most probable isomers in the experiments. [b]The ΔEs are calculated at the CCSD(T)//cc-pVDZ/Si/aug-cc-pVDZ-PP/Nb level of theory. [c]The ADEs and VDEs are calculated at the B3LYP//6-311+G(d)/Si/LanL2DZ/Nb level of theory. [d]The uncertainties of the experimental VDEs and ADEs are ±0.08 eV.

simulated DOS spectrum of isomer 6A can match the experimental peaks centered at 2.98 and 3.82 eV, while that of isomer 6B is in good agreement with the experimental peaks centered at 2.62 and 3.41 eV. The combination of the DOS spectra of isomers 6A and 6B is in good agreement with the experimental spectrum. The existence of isomers 6C and 6D can be ruled out because they are much higher in energy than isomer 6A by at least 0.32 eV. Therefore, isomers 6A and 6B might coexist in our experiments.

$Nb_2Si_7^-$. The lowest lying isomer of $Nb_2Si_7^-$ (7A) can be described as an additional Si atom face capping the $Nb2Si_3$ rhombus of $Nb_2Si_6^-$. The calculated VDE (2.71 eV) of isomer 7A agrees well with the experimental value (2.71 eV), and its simulated DOS spectrum can duplicate the spectral features of the experimental spectrum. The existence of isomers 7B, 7C, and 7D can be ruled out because they are much higher in energy than isomer 7A by at least 0.48 eV. Thus, isomer 7A is suggested to be the most probable structure detected in our experiments.

$Nb_2Si_8^-$. The most stable isomer of $Nb_2Si_8^-$ (8A) can be viewed as a Si_5 five-membered ring penetrated by the vertical Nb−Nb axle and adding a Si_3 triangle at the bottom. The calculated VDEs (2.99, 3.03, and 2.96 eV) of isomers 8A, 8B, and 8C are all in reasonable agreement with the experimental value (3.08 eV), and that of isomer 8D is calculated to be 2.73 eV. The simulated DOS spectra of isomers 8A, 8B, and 8C are consistent with the experimental peak at 3.08 eV and the high-intensity broad peak in the range of 3.25−4.25 eV, while that of isomer 8D is in reasonable agreement with the low-EBE tail in the range of 2.4−2.8 eV. Isomers 8B, 8C, and 8D are higher in energy than isomer 8A by 0.07, 0.17, and 0.20 eV. Thus, we suggest that isomer 8A is the major one detected in the experiments, and isomers 8B, 8C, and 8D are the minor species contributed to the photoelectron spectrum of $Nb_2Si_8^-$. Multiple isomers coexisting in the experiments can explain why the spectral features of $Nb_2Si_8^-$ are very broad.

$Nb_2Si_9^-$. As the ground state structure of $Nb_2Si_9^-$, isomer 9A can be considered as a Si_4 rhombus and a Si_5 pentagonal ring bridged by the Nb−Nb bond, which is perpendicular to the Si_4 and Si_5 subunits. The calculated VDE (2.97 eV) of isomer 9A is in excellent agreement with the experimental value (2.94 eV), and its simulated DOS spectrum fits the peak positions and patterns of the experimental spectrum very well. The calculated VDE of isomer 9B is 2.66 eV, which is much smaller than the experimental value, and its simulated DOS spectrum is also different from the experimental spectrum. The existence of isomers 9C and 9D can be ruled out because they are much higher in energy than isomer 9A by at least 0.41 eV. Thus, isomer 9A is considered as the most probable structure observed in our experiments.

$Nb_2Si_{10}^-$. The lowest lying isomer of $Nb_2Si_{10}^-$ (10A) can be regarded as deriving from isomer 8A by adding a Si atom to cap the triangle face of $Nb1Si_2$ and an additional Si atom to face cap the folded $Nb2Si_3$ rhombus. The calculated VDE (3.02 eV) of isomer 10A is in excellent agreement with the experimental value (3.07 eV), and its DOS spectrum matches the peak positions and patterns of the experimental spectrum very well. The existence of isomers 10B, 10C, and 10D can be ruled out because they are much higher in energy than isomer 10A by at least 0.38 eV. Therefore, we suggest isomer 10A to be the most probable structure contributing to the photoelectron spectrum of $Nb_2Si_{10}^-$.

$Nb_2Si_{11}^-$. The most stable structure of $Nb_2Si_{11}^-$ (11A) is formed by the upper Si_6 hexagon and the lower Si_5 pentagon

DOI: 10.1021/acs.jpcc.7b01904
J. Phys. Chem. C 2017, 121, 11851−11861

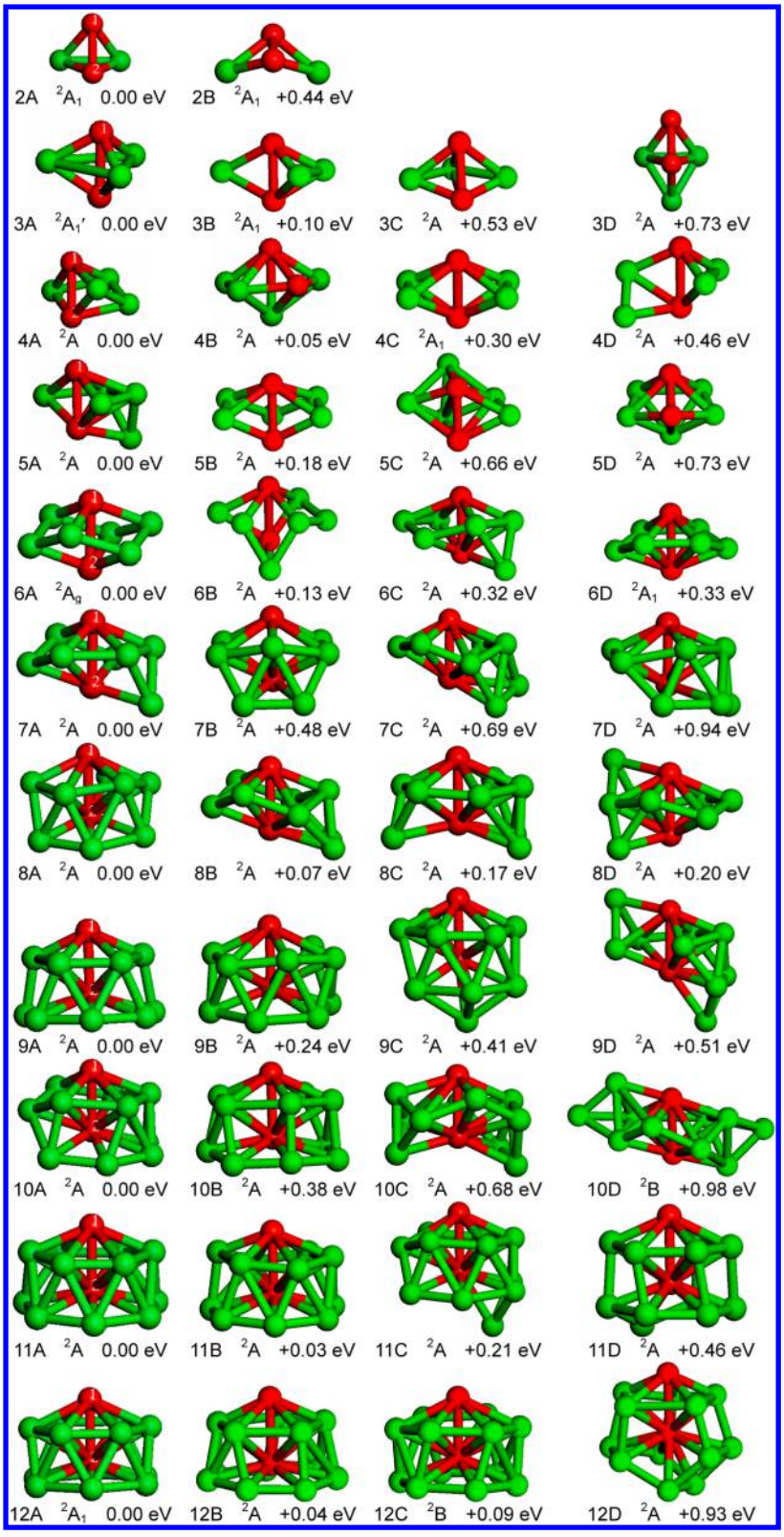

Figure 2. Typical low-lying isomers of anionic $Nb_2Si_n^-$ (n = 2−12) clusters. ΔE values are calculated at the CCSD(T)//cc-pVDZ/Si/aug-cc-pVDZ-PP/Nb level of theory. Green and red balls stand for the Si atoms and Nb atoms, respectively.

interacted with the Nb−Nb bond, which is vertical to the Si_6 and Si_5 subunits. Isomer 11A can also be obtained by two additional Si atoms face capping the upper Si_4 rhombus of isomer 9A. The calculated VDE (3.07 eV) of isomer 11A agrees well with the experimental value (3.09 eV), and its simulated DOS spectrum fits the peak positions and patterns of the experimental spectrum very well. Isomer 11B has a similar structure with its competitive isomer 11A with the upper Si_6 hexagon being slightly distorted. The calculated VDEs (2.96 and 3.00 eV) of isomers 11B and 11C are both in reasonable

DOI: 10.1021/acs.jpcc.7b01904
J. Phys. Chem. C 2017, 121, 11851−11861

Table 2. Bond Lengths of the Most Stable Isomers of $Nb_2Si_n^{-/0}$ (n = 2−12) Clusters

isomer	bond length (Å)	isomer	bond length (Å)
2A	Nb−Nb = 2.37	2A′	Nb−Nb = 2.53
	Nb−Si = 2.50		Nb−Si = 2.40
	Si−Si = 2.71		
3A	Nb−Nb = 2.56	3A′	Nb−Nb = 2.76
	Nb−Si = 2.46		Nb−Si = 2.41
	Si−Si = 3.65		Si−Si = 3.43
4A	Nb−Nb = 2.39	4A′	Nb−Nb = 2.49
	Nb−Si = 2.52−2.67		Nb−Si = 2.45−2.80
	Si−Si = 2.42−2.49		Si−Si = 2.36−2.62
5A	Nb−Nb = 2.43	5A′	Nb−Nb = 2.39
	Nb−Si = 2.57−2.81		Nb−Si = 2.55−2.87
	Si−Si = 2.40−2.51		Si−Si = 2.35−2.45
6A	Nb−Nb = 2.57	6A′	Nb−Nb = 2.52
	Nb−Si = 2.53−2.90		Nb−Si = 2.54−2.95
	Si−Si = 2.44−2.53		Si−Si = 2.32−2.46
7A	Nb−Nb = 2.57	7A′	Nb−Nb = 2.60
	Nb−Si = 2.55−2.97		Nb−Si = 2.51−2.98
	Si−Si = 2.42−2.55		Si−Si = 2.41−2.55
8A	Nb−Nb = 2.52	8A′	Nb−Nb = 2.60
	Nb−Si = 2.52−3.03		Nb−Si = 2.54−2.99
	Si−Si = 2.41−2.97		Si−Si = 2.40−3.32
9A	Nb−Nb = 2.58	9A′	Nb−Nb = 2.68
	Nb−Si = 2.52−2.82		Nb−Si = 2.49−2.90
	Si−Si = 2.35−3.24		Si−Si = 2.30−3.17
10A	Nb−Nb = 2.51	10A′	Nb−Nb = 2.53
	Nb−Si = 2.52−3.04		Nb−Si = 2.53−3.04
	Si−Si = 2.37−3.19		Si−Si = 2.37−3.04
11A	Nb−Nb = 2.53	11A′	Nb−Nb = 2.57
	Nb−Si = 2.61−2.87		Nb−Si = 2.53−3.08
	Si−Si = 2.38−2.76		Si−Si = 2.37−3.09
12A	Nb−Nb = 2.57	12A′	Nb−Nb = 2.95
	Nb−Si = 2.72−2.82		Nb−Si = 2.53−3.08
	Si−Si = 2.45−2.57		Si−Si = 2.37−3.04

agreement with the experimental value, and they are higher in energy than isomer 11A by 0.03 and 0.21 eV. Isomer 11D is unlikely to be detected because it is much higher in energy than isomer 11A by 0.46 eV. Thus, we suggest that isomer 11A is the most probable structure contributing to the experimental spectrum of $Nb_2Si_{11}^-$.

$Nb_2Si_{12}^-$. The most stable isomer of $Nb_2Si_{12}^-$ (12A) is a C_{6v}-symmetric capped hexagonal antiprism with one Nb atom encapsulated inside the Si_{12} cage and the second Nb atom face capping the top of the hexagonal antiprism, similar to the structure of $V_2Si_{12}^-$.[15] Isomer 12A can also be regarded as stemming from isomer 11A by an additional Si atom capping the Si−Si bond of the bottom Si_5 five-membered ring. The VDE of isomer 12A is calculated to be 3.41 eV, which is in excellent agreement with the experimental value (3.45 eV), and its simulated DOS spectrum is in line with the experimental spectrum, although the intensity of the high-EBE part of the DOS spectrum is slightly lower than that of the experimental spectrum. Although isomer 12B is higher in energy than isomer 12A by only 0.04 eV, the existence of isomer 12B can be ruled out because its calculated VDE (2.99 eV) is much smaller than the experimental value. Isomer 12C is higher in energy than isomer 12A by 0.09 eV. The existence of isomer 12D can be ruled out because it is much higher in energy than isomer 12A by 0.93 eV. Therefore, we suggest isomer 12A to be the most likely structure detected in our experiments, and isomer 12C may have a minor contribution to the photoelectron spectrum of $Nb_2Si_{12}^-$. The previous DFT calculations suggested that the structure of $Nb_2Si_{12}^{2-}$ is also a C_{6v}-symmetric capped hexagonal antiprism, similar to isomer 12A.[48]

Nb_2Si_n (n = 2−12) Neutrals. The structures of neutral Nb_2Si_n (n = 2−12) clusters were also optimized at the B3LYP level of theory and are displayed in Figure 4. The most stable structures of neutral Nb_2Si_n generally have similar structural features with their anionic counterparts, except that the structures of Nb_2Si_2, Nb_2Si_4, Nb_2Si_6, Nb_2Si_8, and Nb_2Si_{12} are slightly different from their corresponding anions. The most stable isomer (2A′) of Nb_2Si_2 is a kite-shaped configuration with the two Nb atoms located at the C_2 axis, which is similar to the second isomer (2B) of its anionic counterpart, while the lowest lying isomer (4A′) of Nb_2Si_4 is analogous to isomer 4B of $Nb_2Si_4^-$. The most stable structure (6A′) of Nb_2Si_6 is a capped pentagonal bipyramid, resembling isomer 6C of $Nb_2Si_6^-$. As for Nb_2Si_8, in the most stable isomer (8A′), the eight Si atoms form a bicapped chair-shaped structure with the two capping Si atoms located on the two terminal sides, and the Si_8 unit is penetrated by the vertical Nb−Nb bond. The ground state structure of neutral Nb_2Si_{12} (12A′) can be regarded as one Nb atom sandwiched by a Si_5 five-membered ring and a Si_7 seven-membered ring and with the second Nb atom capping the pentagonal face, which is similar to isomer 12B of $Nb_2Si_{12}^-$. Isomer 12B′ of Nb_2Si_{12} is a C_{2v}-symmetric hexagonal prism structure, which is higher in energy than the ground state structure (12A′) by 0.13 eV at the CCSD(T) level of theory (by 0.02 eV at the B3LYP level of theory). The capped hexagonal antiprism (12C′) of neutral Nb_2Si_{12} is higher in energy than the lowest lying isomer (12A′) by 0.32 eV.

DISCUSSION

The most stable structures of $Nb_2Si_{2-6}^-$ found in this work are in line with the previous theoretical results of $Nb_2Si_n^-$ (n = 2−6).[47] We found that the two Nb atoms in $Nb_2Si_n^{-/0}$ (n = 2−12) clusters tend to stay close to form a Nb−Nb bond, similar to the theoretical results of T_2Si_{1-8} (T = Fe, Co, Ni)[70] and M_2Si_{12} (M = Nb, Ta, Mo, W).[48] The metal−metal bond is also found in our previous works of $V_2Si_{2-6}^{-/0}$ investigated by anion photoelectron spectroscopy and DFT calculations.[54] In addition, the two Nb atoms in $Nb_2Si_n^{-/0}$ prefer to occupy the high coordination sites to form more Nb−Si bonds. That is more likely due to the existence of unfilled d orbitals in the Nb atom. The Nb−Nb bond lengths in $Nb_2Si_n^-$ (n = 2−12) clusters are between 2.37 and 2.68 Å, which are longer than the Nb−Nb bond length of 2.08 Å in the niobium dimer (Nb_2)[71] but shorter than the nearest neighbor distance of 2.86 Å in the metallic niobium.[72] This suggests that there are strong interactions between the two Nb atoms in $Nb_2Si_n^-$ (n = 2−12) clusters. As for neutral Nb_2Si_n clusters, the Nb−Nb distances are in the range of 2.39−2.68 Å at n = 2−11, which are also longer than the Nb−Nb distance in the niobium dimer and shorter than the nearest neighbor distance in the metallic niobium. However, the Nb−Nb distance in neutral Nb_2Si_{12} is about 2.95 Å, which is even longer than the Nb−Nb distance in the metallic niobium. That indicates that the removal of the excess electron from $Nb_2Si_{12}^-$ anion weakens the Nb−Nb bond (which can be confirmed by the analyses of molecular orbitals).

It is interesting to compare the structures of $Nb_2Si_n^-$ with those of $V_2Si_n^-$. The structures of $V_2Si_{3-6}^-$ have been reported by Xu et al.[54] and $V_2Si_{12}^-$ reported by Huang et al.[15] At n = 3−

DOI: 10.1021/acs.jpcc.7b01904
J. Phys. Chem. C 2017, 121, 11851−11861

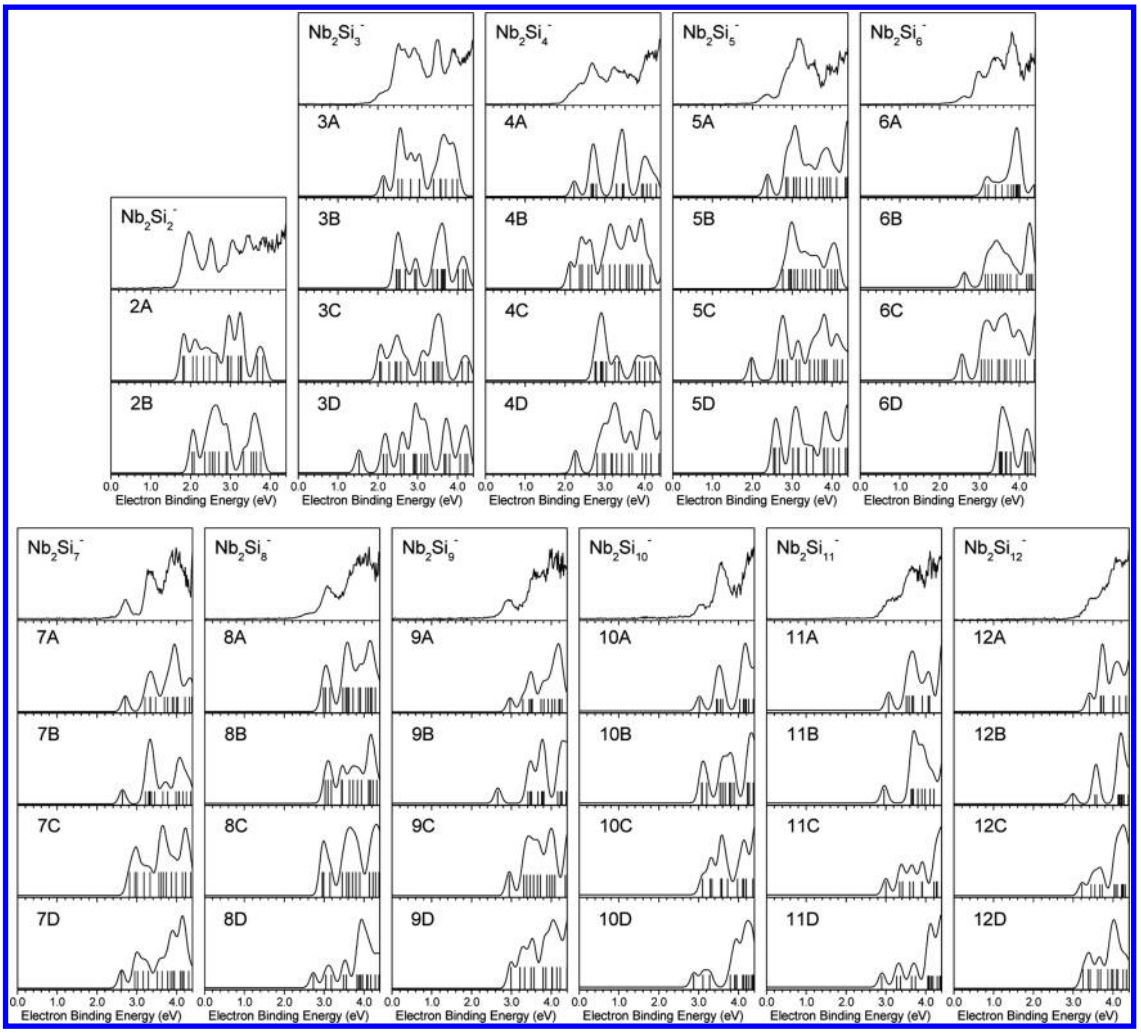

Figure 3. Comparison between the experimental photoelectron spectra and the simulated DOS spectra of the low-lying isomers of $Nb_2Si_n^-$ (n = 2−12) clusters. Simulated spectra were obtained by fitting the distribution of the transition lines with the unit area Gaussian functions of 0.20 eV full widths at half-maximum.

6, the photoelectron spectra of $Nb_2Si_n^-$ are similar to those of $V_2Si_n^-$ except that the VDEs of $Nb_2Si_n^-$ are slightly lower than those of $V_2Si_n^-$. The most stable isomers of $Nb_2Si_n^-$ and $V_2Si_n^-$ are all regarded as the metals face capping the Si_n frameworks and occupying the high coordination sites. Their similar geometric structures can explain why $Nb_2Si_n^-$ and $V_2Si_n^-$ have similar spectral features. The Si_6 chair-shaped structure of $Nb_2Si_6^-$ is slightly distorted to the lower C_{2h} symmetry compared to the D_{3d} symmetry of $V_2Si_6^-$, and the Si−Si bond lengths (2.42−2.55 Å) in $Nb_2Si_6^-$ are longer than those (2.38−2.44 Å) in $V_2Si_6^-$, probably because the atomic radius of the Nb atom (1.47 Å) is larger than that of the V atom (1.35 Å). At n = 12, the spectral feature of $Nb_2Si_{12}^-$ is also similar to that of $V_2Si_{12}^-$, but the experimental VDE of $Nb_2Si_{12}^-$ is lower than that of $V_2Si_{12}^-$ by 0.21 eV. The global minima of both $Nb_2Si_{12}^-$ and $V_2Si_{12}^-$ are a capped hexagonal antiprism with one metal atom encapsulated into the Si_{12} cage and the other metal atom face capping the top of the hexagonal antiprism. The height and sides (2.57 and 2.45 Å) of $Nb_2Si_{12}^-$-capped hexagonal antiprism are slightly longer than those (2.53 and 2.43 Å) of $V_2Si_{12}^-$, which is because the atomic radius of the Nb atom is larger than that of the V atom.

To give insight into the charge distributions of $Nb_2Si_n^-$ clusters, we conducted the atomic dipole moment-corrected Hirshfeld population (ADCH) analyses on the most stable isomers of $Nb_2Si_n^-$ (n = 2−12) clusters and presented them in Figure 5. The ADCH charge on the Nb1 atom ranges from −0.12 e to 0.45 e, while that on the Nb2 atom is in the range of −0.12 e to 0.34 e. The ADCH charge distributions on the two Nb atoms are very similar at n = 2−6 and display no significant changes, which is probably due to the two Nb atoms interacting with nearly the same number of Si atoms in these clusters. For cluster sizes of n = 7−12, the two Nb atoms begin to bond with different number of Si atoms, resulting in the different ADCH charge distributions on the two Nb atoms. In particular, at n = 12, the ADCH charge on the Nb1 atom is 0.45 e and that on the Nb2 atom is 0.06 e, more likely related to the formation of a C_{6v}-symmetric capped hexagonal antiprism. Except for $Nb_2Si_2^-$, the ADCH charge distributions on the two Nb atoms are positive values, which is more likely due to the electronegativity of the Si atom (χ = 1.90) being stronger than that of the Nb atom (χ = 1.60).[73] This also implies that there is slight charge transfer from the two Nb atoms to the Si_n frameworks. It seems that the ADCH charge distributions on the two Nb atoms are associated with the structural evolution of $Nb_2Si_n^-$ clusters and the electronegativities of the Si and Nb atoms.

To further understand the bonding nature in $Nb_2Si_n^-$ clusters, we calculated the Wiberg bond orders and Mayer

DOI: 10.1021/acs.jpcc.7b01904
J. Phys. Chem. C 2017, 121, 11851−11861

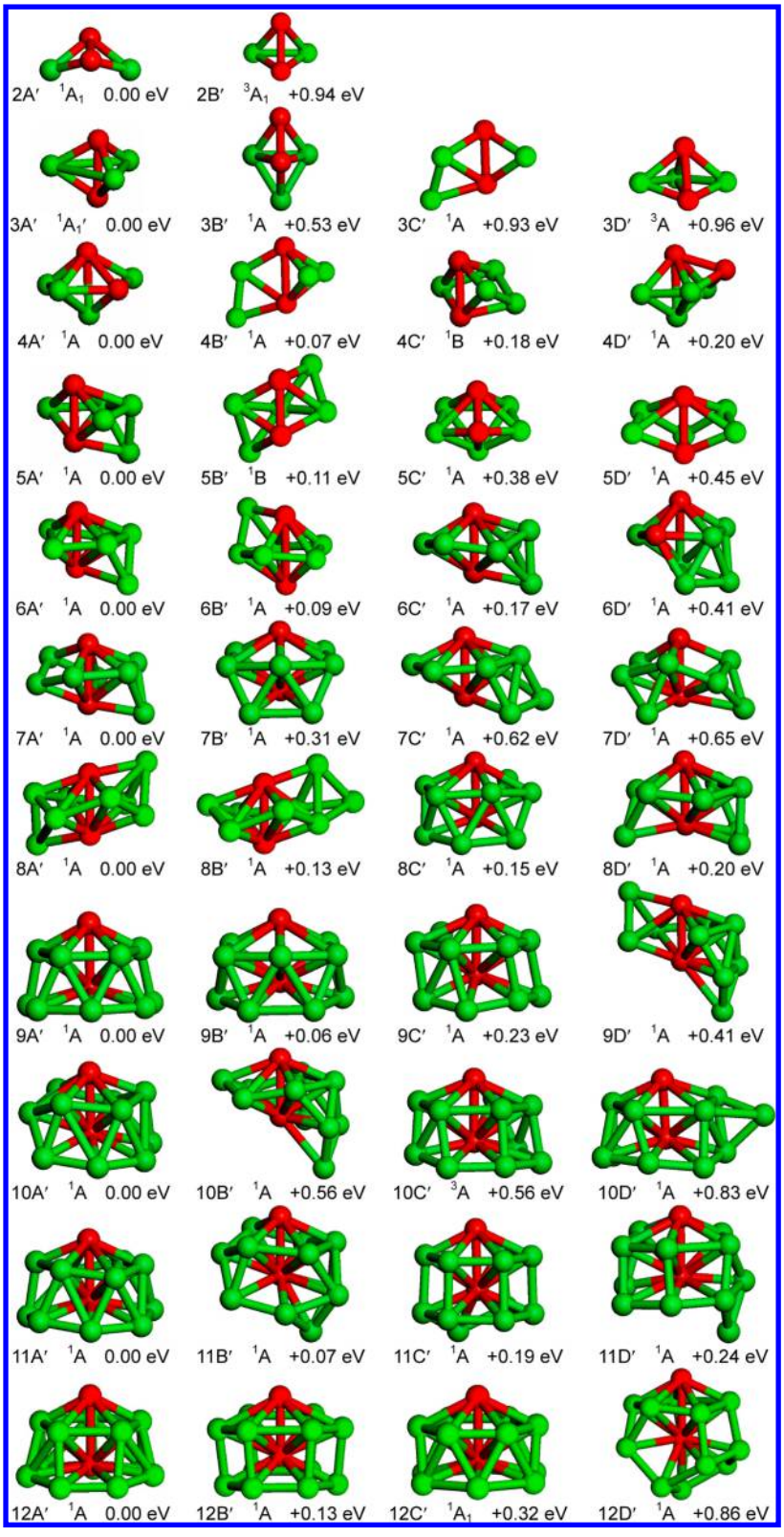

Figure 4. Typical low-lying isomers of neutral Nb_2Si_n (n = 2−12) clusters. ΔE values are calculated at the CCSD(T)//cc-pVDZ/Si/aug-cc-pVDZ-PP/Nb level of theory. Green and red balls stand for the Si atoms and Nb atoms, respectively.

bond orders of the chemical bonds in $Nb_2Si_3^-$, $Nb_2Si_6^-$, and $Nb_2Si_{12}^-$. The calculations show that the Wiberg bond orders of the Nb−Nb bonds in $Nb_2Si_3^-$, $Nb_2Si_6^-$, and $Nb_2Si_{12}^-$ are 2.05, 1.71, and 1.47, respectively, whereas the Mayer bond orders are 1.89, 1.87, and 1.39, respectively. The high Nb−Nb bond orders reveal that the interactions between the two Nb atoms are very strong in these clusters. We also conducted detailed analyses on the molecular orbitals of $Nb_2Si_3^-$, $Nb_2Si_6^-$, and $Nb_2Si_{12}^-$ and presented them in Figure 6. From Figure 6 it can be seen that the singly occupied molecular orbital (SOMO)

DOI: 10.1021/acs.jpcc.7b01904
J. Phys. Chem. C 2017, 121, 11851−11861

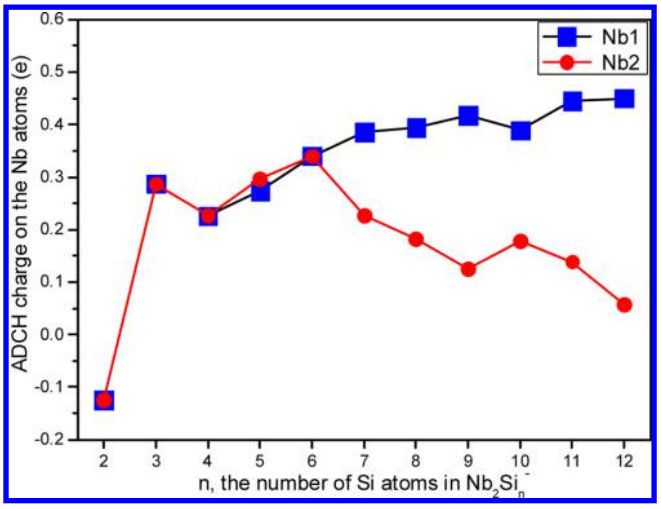

Figure 5. ADCH charge on the two Nb atoms of the most stable isomers of $Nb_2Si_n^-$ (n = 2−12) clusters.

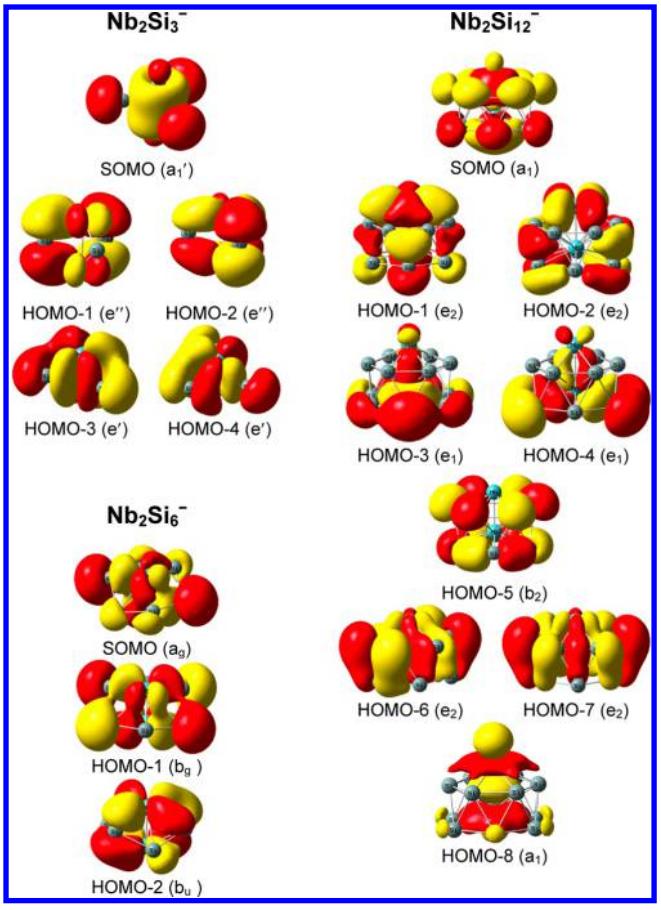

Figure 6. Molecular orbitals of $Nb_2Si_3^-$, $Nb_2Si_6^-$, and $Nb_2Si_{12}^-$ anions (isosurface value = 0.02). For each cluster, the orbitals in the same row are energetically degenerate.

of $Nb_2Si_3^-$ displays a large overlap between the $4d_{z^2}$ orbitals of the Nb atoms. From the HOMO-3 and HOMO-4 of $Nb_2Si_3^-$ it can be seen that there are large overlaps between the $4d_{xy}$ and the $4d_{x^2-y^2}$ orbitals of the Nb atoms, respectively. The SOMO and HOMO-1 of $Nb_2Si_6^-$ show large overlaps between the $4d_{xy}$ and the $4d_{x^2-y^2}$ orbitals of the Nb atoms, respectively. As for $Nb_2Si_{12}^-$, the SOMO and HOMO-8 reveal large overlaps between the $4d_{z^2}$ orbitals of the Nb atoms, the HOMO-3 and HOMO-4 display overlaps between the $4d_{xz}$ and $4d_{yz}$ of the Nb atoms, respectively, and the HOMO-6 and HOMO-7 show overlaps between the $4d_{xy}$ and the $4d_{x^2-y^2}$ orbitals of the Nb atoms, respectively. The strong interactions between the 4d orbitals of the two Nb atoms are consistent with the high Nb−Nb bond orders and the short Nb−Nb bond lengths (2.37−2.68 Å) found in $Nb_2Si_n^-$ clusters. It is also worth mentioning that the SOMOs of $Nb_2Si_3^-$, $Nb_2Si_6^-$, and $Nb_2Si_{12}^-$ are mainly composed by the 4d orbitals of the Nb atoms and the 3s3p hybridized orbitals of the Si_n frameworks, and the electron densities are delocalized over the whole clusters, suggesting that there are delocalized Nb_2-Si_n ligand interactions between the Nb atoms and the Si_n frameworks. Overall, the strong Nb−Nb bonds and the delocalized Nb_2-Si_n ligand interactions play important roles in the stability of the D_{3h}-symmetric trigonal bipyramid structure of $Nb_2Si_3^-$, the C_{2h}-symmetric Si_6 chair-shaped structure of $Nb_2Si_6^-$, and the C_{6v}-symmetric capped hexagonal antiprism of $Nb_2Si_{12}^-$.

CONCLUSIONS

We conducted a combined anion photoelectron spectroscopy and theoretical study on bi-Nb-doped silicon clusters. We found that the two Nb atoms in $Nb_2Si_n^{-/0}$ (n = 2−12) clusters tend to stay close to form a Nb−Nb bond and occupy the high coordination sites to interact with more Si atoms. The most stable structures of $Nb_2Si_n^{-/0}$ (n = 2−12) clusters can be regarded as a central axis of Nb_2 surrounded by the Si atoms. The most stable isomers of $Nb_2Si_n^-$ anions are all in spin doublet states, while those of the neutral clusters are all in spin singlet states. The most stable isomers of anionic and neutral Nb_2Si_3 are D_{3h}-symmetric trigonal bipyramid structures, that of $Nb_2Si_6^-$ has C_{2h} symmetry with the six Si atoms forming a chair-shaped structure, and that of $Nb_2Si_{12}^-$ has a C_{6v}-symmetric capped hexagonal antiprism structure. According to the atomic dipole moment-corrected Hirshfeld population (ADCH) analyses, the ADCH charge distributions on the two Nb atoms are not only associated with the structural evolution of $Nb_2Si_n^-$ clusters but also related to the electronegativities of Si and Nb atoms. Additionally, we analyzed the molecular orbitals of $Nb_2Si_3^-$, $Nb_2Si_6^-$, and $Nb_2Si_{12}^-$ anions and confirmed that the strong Nb−Nb bonds and the delocalized Nb_2-Si_n ligand interactions are important for their structural stability. The current study may provide insights into the structural and bonding properties of Nb−Si-based films and alloys at the molecular level.

ASSOCIATED CONTENT

Supporting Information

The Supporting Information is available free of charge on the ACS Publications website at DOI: 10.1021/acs.jpcc.7b01904.

Cartesian coordinates of the low-lying isomers of $Nb_2Si_n^{-/0}$ (n = 2−12) clusters (PDF)

AUTHOR INFORMATION

Corresponding Authors

*E-mail: xuhong@iccas.ac.cn. Phone: +86 10 62563168. Fax: +86 10 62563167.

*E-mail: xlxu@iccas.ac.cn. Phone: +86 10 62563168. Fax: +86 10 62563167.

*E-mail: zhengwj@iccas.ac.cn. Phone: +86 10 62635054. Fax: +86 10 62563167.

DOI: 10.1021/acs.jpcc.7b01904
J. Phys. Chem. C 2017, 121, 11851−11861

ORCID
Wei-Jun Zheng: 0000-0002-9136-2693

Notes

The authors declare no competing financial interest.

■ ACKNOWLEDGMENTS

This work was supported by the National Natural Science Foundation of China (Grant Nos. 21273246 and 21103202) and the Chinese Academy of Sciences (Grant No. QYZDB-SSW-SLH024). The theoretical calculations were performed on the China Scientific Computing Grid (ScGrid) of the Supercomputing Center, Computer Network Information Center of the Chinese Academy of Sciences.

■ REFERENCES

(1) Zhang, B. H.; Wang, H. S.; Lu, L. H.; Ai, K. L.; Zhang, G.; Cheng, X. L. Large-area silver-coated silicon nanowire arrays for molecular sensing using surface-enhanced raman spectroscopy. *Adv. Funct. Mater.* **2008**, *18*, 2348−2355.
(2) Reece, S. Y.; Hamel, J. A.; Sung, K.; Jarvi, T. D.; Esswein, A. J.; Pijpers, J. J. H.; Nocera, D. G. Wireless solar water splitting using silicon-based semiconductors and earth-abundant catalysts. *Science* **2011**, *334*, 645−648.
(3) Nakao, Y.; Hiyama, T. Silicon-based cross-coupling reaction: an environmentally benign version. *Chem. Soc. Rev.* **2011**, *40*, 4893−4901.
(4) Su, X.; Wu, Q. L.; Li, J. C.; Xiao, X. C.; Lott, A.; Lu, W. Q.; Sheldon, B. W.; Wu, J. Silicon-based nanomaterials for lithium-ion batteries: a review. *Adv. Energy Mater.* **2014**, *4*, 1300882.
(5) Ji, L.; McDaniel, M. D.; Wang, S. J.; Posadas, A. B.; Li, X. H.; Huang, H. Y.; Lee, J. C.; Demkov, A. A.; Bard, A. J.; Ekerdt, J. G.; et al. A silicon-based photocathode for water reduction with an epitaxial $SrTiO_3$ protection layer and a nanostructured catalyst. *Nat. Nanotechnol.* **2015**, *10*, 84−90.
(6) Kaiser, B.; Calvet, W.; Murugasen, E.; Ziegler, J.; Jaegermann, W.; Pust, S. E.; Finger, F.; Hoch, S.; Blug, M.; Busse, J. Light induced hydrogen generation with silicon-based thin film tandem solar cells used as photocathode. *Int. J. Hydrogen Energy* **2015**, *40*, 899−904.
(7) Bogdanoff, P.; Stellmach, D.; Gabriel, O.; Stannowski, B.; Schlatmann, R.; van de Krol, R.; Fiechter, S. Artificial leaf for water splitting based on a triple-junction thin-film silicon solar cell and a pedot: pss/catalyst blend. *Energy Technol.* **2016**, *4*, 230−241.
(8) Andriotis, A. N.; Mpourmpakis, G.; Froudakis, G. E.; Menon, M. Stabilization of Si-based cage clusters and nanotubes by encapsulation of transition metal atoms. *New J. Phys.* **2002**, *4*, 78.
(9) Reis, C. L.; Martins, J. L.; Pacheco, J. M. Stability analysis of a bulk material built from silicon cage clusters: a first-principles approach. *Phys. Rev. B: Condens. Matter Mater. Phys.* **2007**, *76*, 233406.
(10) Claridge, S. A.; Castleman, A. W.; Khanna, S. N.; Murray, C. B.; Sen, A.; Weiss, P. S. Cluster-assembled materials. *ACS Nano* **2009**, *3*, 244−255.
(11) Berkdemir, C.; Gülseren, O. First-principles investigation of pentagonal and hexagonal core-shell silicon nanowires with various core compositions. *Phys. Rev. B: Condens. Matter Mater. Phys.* **2009**, *80*, 115334.
(12) Liu, Z. F.; Wang, X. Q.; Cai, J. T.; Zhu, H. J. Room-temperature ordered spin structures in cluster-assembled single $V@Si_{12}$ sheets. *J. Phys. Chem. C* **2015**, *119*, 1517−1523.
(13) Wang, J.; Liu, J. H. Investigation of size-selective $Zr_2@Si_n$ (n = 16−24) caged clusters. *J. Phys. Chem. A* **2008**, *112*, 4562−4567.
(14) Ji, W. X.; Luo, C. L. Structures, magnetic properties, and electronic counting rule of metals-encapsulated cage-like M_2Si_{18} (M = Ti-Zn) clusters. *Int. J. Quantum Chem.* **2012**, *112*, 2525−2531.
(15) Huang, X. M.; Xu, H. G.; Lu, S. J.; Su, Y.; King, R. B.; Zhao, J. J.; Zheng, W. J. Discovery of a silicon-based ferrimagnetic wheel structure in $V_xSi_{12}^-$ (x = 1−3) clusters: photoelectron spectroscopy and density functional theory investigation. *Nanoscale* **2014**, *6*, 14617−14621.
(16) Xu, H. G.; Kong, X. Y.; Deng, X. J.; Zhang, Z. G.; Zheng, W. J. Smallest fullerene-like silicon cage stabilized by a V_2 unit. *J. Chem. Phys.* **2014**, *140*, 024308.
(17) Zhao, R.-N.; Han, J.-G.; Duan, Y.-H. Density functional theory investigations on the geometrical and electronic properties and growth patterns of Si_n (n = 10−20) clusters with bimetal Pd_2 impurities. *Thin Solid Films* **2014**, *556*, 571−579.
(18) Hagelberg, F.; Xiao, C.; Lester, W. A. Cagelike Si_{12} clusters with endohedral Cu, Mo, and W metal atom impurities. *Phys. Rev. B: Condens. Matter Mater. Phys.* **2003**, *67*, 035426.
(19) Singh, A. K.; Briere, T. M.; Kumar, V.; Kawazoe, Y. Magnetism in transition-metal-doped silicon nanotubes. *Phys. Rev. Lett.* **2003**, *91*, 146802.
(20) Robles, R.; Khanna, S.; Castleman, A. Stability and magnetic properties of T_2Si_n (T = Cr, Mn, $1 \leqslant n \leqslant 8$) clusters. *Phys. Rev. B: Condens. Matter Mater. Phys.* **2008**, *77*, 235441.
(21) Iwasa, T.; Nakajima, A. Geometric, electronic, and optical properties of a superatomic heterodimer and trimer: $Sc@Si_{16}$−$V@Si_{16}$ and $Sc@Si_{16}$−$Ti@Si_{16}$−$V@Si_{16}$. *J. Phys. Chem. C* **2012**, *116*, 14071−14077.
(22) Palagin, D.; Teufl, T.; Reuter, K. Multidoping of Si cages: high spin states beyond the single-dopant septet limit. *J. Phys. Chem. C* **2013**, *117*, 16182−16186.
(23) Aubin, H.; Marrache-Kikuchi, C. A.; Pourret, A.; Behnia, K.; Bergé, L.; Dumoulin, L.; Lesueur, J. Magnetic-field-induced quantum superconductor-insulator transition in $Nb_{0.15}Si_{0.85}$. *Phys. Rev. B: Condens. Matter Mater. Phys.* **2006**, *73*, 094521.
(24) Lefranc, S.; Piat, M.; Torre, J. P.; Bréelle, E.; Leriche, B.; Dumoulin, L.; Bergé, L.; Evesque, C.; Pajot, F. Superconducting NbSi thermometers for use in tes devices. *Nucl. Instrum. Methods Phys. Res., Sect. A* **2006**, *559*, 468−470.
(25) Olaya, D.; Dresselhaus, P. D.; Benz, S. P. Niobium-silicide junction technology for superconducting digital electronics. *Ieice. Trans. Electron.* **2010**, *E93-C*, 463−467.
(26) Crauste, O.; Gentils, A.; Couëdo, F.; Dolgorouky, Y.; Bergé, L.; Collin, S.; Marrache-Kikuchi, C. A.; Dumoulin, L. Effect of annealing on the superconducting properties of a-Nb_xSi_{1-x} thin films. *Phys. Rev. B: Condens. Matter Mater. Phys.* **2013**, *87*, 144514.
(27) Marrache-Kikuchi, C. A.; Berge, L.; Collin, S.; Dobrea, C.; Dumoulin, L.; Juillard, A.; Marnieros, S. Properties of thermometric NbSi thin films and application to detection in astrophysics. *Nucl. Instrum. Methods Phys. Res., Sect. A* **2006**, *559*, 579−581.
(28) Bewlay, B. P.; Jackson, M. R.; Lipsitt, H. A. The balance of mechanical and environmental properties of a multielement niobium-niobium silicide-based in situ composite. *Metall. Mater. Trans. A* **1996**, *27*, 3801−3808.
(29) Marnieros, S.; Berge, L.; Broniatowski, A.; Chapellier, M.; Collin, S.; Crauste, O.; Defay, X.; Dolgorouky, Y.; Dumoulin, L.; Juillard, A.; et al. Surface event rejection of the edelweiss cryogenic germanium detectors based on NbSi thin film sensors. *J. Low Temp. Phys.* **2008**, *151*, 835−840.
(30) Crauste, O.; Marrache-Kikuchi, C. A.; Bergé, L.; Stanescu, D.; Dumoulin, L. Thickness dependence of the superconductivity in thin disordered NbSi films. *J. Phys.: Conf. Ser.* **2009**, *150*, 042019.
(31) Crauste, O.; Marrache-Kikuchi, C. A.; Bergé, L.; Collin, S.; Dolgorouky, Y.; Marnieros, S.; Nones, C.; Dumoulin, L. Tunable superconducting properties of a-NbSi thin films and application to detection in astrophysics. *J. Low Temp. Phys.* **2011**, *163*, 60−66.
(32) Proslier, T.; Klug, J. A.; Elam, J. W.; Claus, H.; Becker, N. G.; Pellin, M. J. Atomic layer deposition and superconducting properties of NbSi films. *J. Phys. Chem. C* **2011**, *115*, 9477−9485.
(33) Wei, W. Q.; Wang, H. W.; Zou, C. M.; Zhu, Z. J.; Wei, Z. J. Microstructure and oxidation behavior of Nb-based multi-phase alloys. *Mater. Eng.* **2013**, *46*, 1−7.
(34) Pan, Y.; Lin, Y. H.; Xue, Q.; Ren, C. Q.; Wang, H. Relationship between Si concentration and mechanical properties of Nb−Si compounds: a first−principles study. *Mater. Des.* **2016**, *89*, 676−683.

DOI: 10.1021/acs.jpcc.7b01904
J. Phys. Chem. C 2017, 121, 11851−11861

(35) Wang, W.; Zhou, C. G. Hot corrosion behaviour of Nb_{ss}/Nb_5Si_3 in situ composites in the mixture of Na_2SO_4 and NaCl melts. *Corros. Sci.* **2013**, *74*, 345−352.
(36) Kang, Y. W.; Yan, Y. C.; Song, J. X.; Ding, H. S. Microstructures and mechanical properties of Nb_{ss}/Nb_5Si_3 in-situ composite prepared by electromagnetic cold crucible directional solidification. *Mater. Sci. Eng., A* **2014**, *599*, 87−91.
(37) Xiong, B. W.; Cai, C. C.; Wang, Z. J. Microstructures and room temperature fracture toughness of Nb/Nb_5Si_3 composites alloyed with W, Mo and W−Mo fabricated by spark plasma sintering. *J. Alloys Compd.* **2014**, *604*, 211−216.
(38) Yan, Y. C.; Ding, H. S.; Kang, Y. W.; Song, J. X. Microstructure evolution and mechanical properties of Nb−Si based alloy processed by electromagnetic cold crucible directional solidification. *Mater. Eng.* **2014**, *55*, 450−455.
(39) Pan, Y.; Lin, Y.-H.; Wang, H.; Zhang, C.-M. Vacancy induced brittle−to−ductile transition of Nb_5Si_3 alloy from first−principles. *Mater. Des.* **2015**, *86*, 259−265.
(40) Shi, S. X.; Zhu, L. G.; Jia, L. N.; Zhang, H.; Sun, Z. M. Ab−initio study of alloying effects on structure stability and mechanical properties of α−Nb_5Si_3. *Comput. Mater. Sci.* **2015**, *108*, 121−127.
(41) Pacheco, J.; Gueorguiev, G.; Martins, J. First-principles study of the possibility of condensed phases of endohedral silicon cage clusters. *Phys. Rev. B: Condens. Matter Mater. Phys.* **2002**, *66*, 033401.
(42) Sen, P.; Mitas, L. Electronic structure and ground states of transition metals encapsulated in a Si_{12} hexagonal prism cage. *Phys. Rev. B: Condens. Matter Mater. Phys.* **2003**, *68*, 155404.
(43) Gueorguiev, G. K.; Pacheco, J. M.; Stafström, S.; Hultman, L. Silicon−metal clusters: nano-templates for cluster assembled materials. *Thin Solid Films* **2006**, *515*, 1192−1196.
(44) Xia, X. X.; Hermann, A.; Kuang, X. Y.; Jin, Y. Y.; Lu, C.; Xing, X. D. Study of the structural and electronic properties of neutral and charged niobium-doped silicon clusters: niobium encapsulated in silicon cages. *J. Phys. Chem. C* **2016**, *120*, 677−684.
(45) Li, X. J.; Yan, Z. J.; Li, S. N. The nature of structure and bonding between transition metal and mixed Si-Ge tetramers: a 20-electron superatom system. *J. Comput. Chem.* **2016**, *37*, 2316−2323.
(46) Li, X. J.; Han, Q.; Yang, X. H.; Song, R. J.; Song, L. M. Modification of alkali metals on silicon-based nanoclusters: an enhanced nonlinear optical response. *Chem. Phys. Lett.* **2016**, *659*, 93−99.
(47) Ru, H.; Ping, G.; Yong-Zhuang, C.; Ji-Liang, Z.; Shu-Ting, L.; Zhao-Yu, R. A density functional investigation of $Nb_2Si_n^-$ (n = 1−6) clusters. *J. Atom. Mol. Phys.* **2014**, *31*, 385.
(48) Pham, H. T.; Majumdar, D.; Leszczynski, J.; Nguyen, M. T. 4d and 5d bimetal doped tubular silicon clusters $Si_{12}M_2$ with M = Nb, Ta, Mo and W: a bimetallic configuration model. *Phys. Chem. Chem. Phys.* **2017**, *19*, 3115−3124.
(49) Gunaratne, K. D.; Berkdemir, C.; Harmon, C. L.; Castleman, A. W. Probing the valence orbitals of transition metal-silicon diatomic anions: ZrSi, NbSi, MoSi, PdSi and WSi. *Phys. Chem. Chem. Phys.* **2013**, *15*, 6068−6079.
(50) Koyasu, K.; Atobe, J.; Furuse, S.; Nakajima, A. Anion photoelectron spectroscopy of transition metal- and lanthanide metal-silicon clusters: MSi_n^- (n = 6−20). *J. Chem. Phys.* **2008**, *129*, 214301.
(51) Lu, S. J.; Cao, G. J.; Xu, X. L.; Xu, H. G.; Zheng, W. J. The structural and electronic properties of $NbSi_n^{-/0}$ (n = 3−12) clusters: anion photoelectron spectroscopy and ab initio calculations. *Nanoscale* **2016**, *8*, 19769−19778.
(52) Koyasu, K.; Atobe, J.; Akutsu, M.; Mitsui, M.; Nakajima, A. Electronic and geometric stabilities of clusters with transition metal encapsulated by silicon. *J. Phys. Chem. A* **2007**, *111*, 42−49.
(53) Li, X. J.; Claes, P.; Haertelt, M.; Lievens, P.; Janssens, E.; Fielicke, A. Structural determination of niobium-doped silicon clusters by far-infrared spectroscopy and theory. *Phys. Chem. Chem. Phys.* **2016**, *18*, 6291−6300.
(54) Xu, H.-G.; Zhang, Z.-G.; Feng, Y.; Yuan, J. Y.; Zhao, Y. C.; Zheng, W. J. Vanadium-doped small silicon clusters: photoelectron spectroscopy and density-functional calculations. *Chem. Phys. Lett.* **2010**, *487*, 204−208.
(55) Lee, C.; Yang, W.; Parr, R. G. Development of the colle-salvetti correlation-energy formula into a functional of the electron density. *Phys. Rev. B: Condens. Matter Mater. Phys.* **1988**, *37*, 785−789.
(56) Becke, A. D. Density-functional thermochemistry. III. The role of exact exchange. *J. Chem. Phys.* **1993**, *98*, 5648−5652.
(57) Frisch, M. J.; Trucks, G. W.; Schlegel, H. B.; Scuseria, G. E.; Robb, M. A.; Cheeseman, J. R.; Scalmani, G.; Barone, V.; Mennucci, B.; Peterson, K. A.; et al. *Gaussian 09, Revision A.02*; Gaussian, Inc.: Wallingford, CT, 2009.
(58) Hay, P. J.; Wadt, W. R. Ab initio effective core potentials for molecular calculations. Potentials for the transition metal atoms Sc to Hg. *J. Chem. Phys.* **1985**, *82*, 270−283.
(59) McLean, A. D.; Chandler, G. S. Contracted gaussian basis sets for molecular calculations. I. Second row atoms, Z = 11−18. *J. Chem. Phys.* **1980**, *72*, 5639−5648.
(60) Lv, J.; Wang, Y. C.; Zhu, L.; Ma, Y. M. Particle-swarm structure prediction on clusters. *J. Chem. Phys.* **2012**, *137*, 084104.
(61) Scuseria, G. E.; Schaefer, H. F. Is coupled cluster singles and doubles (CCSD) more computationally intensive than quadratic configuration interaction (QCISD)? *J. Chem. Phys.* **1989**, *90*, 3700−3703.
(62) Purvis, G. D.; Bartlett, R. J. A full coupled - cluster singles and doubles model: the inclusion of disconnected triples. *J. Chem. Phys.* **1982**, *76*, 1910−1918.
(63) Peterson, K. A.; Figgen, D.; Dolg, M.; Stoll, H. Energy-consistent relativistic pseudopotentials and correlation consistent basis sets for the 4d elements Y-Pd. *J. Chem. Phys.* **2007**, *126*, 124101.
(64) Woon, D. E.; Dunning, T. H. Gaussian basis sets for use in correlated molecular calculations. III. The atoms aluminum through argon. *J. Chem. Phys.* **1993**, *98*, 1358−1371.
(65) Lu, T.; Chen, F. W. Multiwfn: a multifunctional wavefunction analyzer. *J. Comput. Chem.* **2012**, *33*, 580−592.
(66) Lu, T.; Chen, F. W. Atomic dipole moment corrected hirshfeld population method. *J. Theor. Comput. Chem.* **2012**, *11*, 163−183.
(67) Lu, T.; Chen, F. W. Comparison of computational methods for atomic charges. *Acta Phys.-Chim. Sin.* **2012**, *28*, 1−18.
(68) Tozer, D. J.; Handy, N. C. Improving virtual kohn−sham orbitals and eigenvalues: application to excitation energies and static polarizabilities. *J. Chem. Phys.* **1998**, *109*, 10180−10189.
(69) Akola, J.; Manninen, M.; Häkkinen, H.; Landman, U.; Li, X.; Wang, L. S. Photoelectron spectra of aluminum cluster anions: temperature effects and ab initio simulations. *Phys. Rev. B: Condens. Matter Mater. Phys.* **1999**, *60*, 297−300.
(70) Robles, R.; Khanna, S. N. Stable T_2Si_n (T = Fe, Co, Ni, n = 1- 8) cluster motifs. *J. Chem. Phys.* **2009**, *130*, 164313.
(71) James, A. M.; Kowalczyk, P.; Fournier, R.; Simard, B. Electronic spectroscopy of the niobium dimer molecule: experimental and theoretical results. *J. Chem. Phys.* **1993**, *99*, 8504−8518.
(72) Wyckoff, R. W. G. *Crystal Structures*; Interscience: New York., 1963.
(73) Pauling, L. The energy of single bonds and the relative electronegativity of atoms. *J. Am. Chem. Soc.* **1932**, *54*, 3570−3582.

DOI: 10.1021/acs.jpcc.7b01904
J. Phys. Chem. C 2017, 121, 11851−11861